Tellus SERIES A DYNAMIC METEOROLOGY AND OCEANOGRAPHY
PUBLISHED BY THE INTERNATIONAL METEOROLOGICAL INSTITUTE IN STOCKHOLM

Impact of different cumulus convective parameterization schemes on the simulation of precipitation over China

By DANLIAN HUANG and SHIBO GAO*, *School of Atmospheric Sciences, Nanjing University of Information Science and Technology, Nanjing, China*

(Manuscript received 15 May 2017; in final form 11 November 2017)

ABSTRACT

The impact of two cumulus convective schemes on the simulation of the precipitation over China is investigated using the Weather Research and Forecasting (WRF) model. Simulations for the period of 1982–2004 are performed at a horizontal resolution of 30 km and forced by NCEP Reanalysis II data. Results show precipitation simulated with the WRF model is quite sensitive to the choice of Kain–Fritsch and Grell cumulus schemes. Both the schemes have distinct skills in predicting the seasonal mean pattern, annual cycle and interannual variation in precipitation. The results show that the Kain–Fritsch scheme tends to overestimate the magnitude of the summer and annual mean precipitation over the main rain-belts, while the Grell scheme tends to underestimate these effects, particularly the simulation of the summer extreme precipitation. However, the Kain–Fritsch scheme is more skilful in capturing the seasonal mean pattern and annual cycle with higher spatial correlations in the main rain-belts. The Grell scheme shows some advantages for northern China and the Tibetan Plateau, especially in representing the interannual variation. The optimal ensemble approach is used to determine the best combination of the two schemes, with the results giving a better overall performance than the individual schemes alone in predicting summer precipitation. The temporal correlation coefficient of precipitation for the ensemble is significantly higher, while the root mean square error of extreme precipitation is reduced compared with the Kain–Fritsch and Grell results. This shows that the ensemble approach based on the optimal ensemble weight combines the advantages of the two cumulus schemes efficiently.

Keywords: WRF model, Kain–Fritsch cumulus scheme, Grell cumulus scheme, ensemble downscaling

1. Introduction

General circulation models (GCMs) have proven to be capable of simulating large-scale circulation and the global climate, but are limited in resolving regional-scale features of the climate, especially in the accurate simulation of precipitation (Kang et al., 2002; Zhou and Yu, 2006; Zhou et al., 2008; Huang et al., 2013; Kitoh et al., 2013). A more applicable technique is dynamic downscaling, which uses regional climate models (RCMs) forced by global reanalysis data or GCMs. It is widely accepted that RCMs can improve the simulation of precipitation compared with GCMs, because of the more comprehensive representation of the important physical processes at a finer resolution (Giorgi and Bates, 1989; Giorgi and Mearns, 1999; Cocke et al., 2007; Gao et al., 2012; Gao et al., 2017).

However, it is still a significant challenge for RCMs to accurately represent the characteristics of precipitation, arising from the complexity of representing the physical processes of precipitation, including cumulus convection, planetary boundry-layer turbulence, cloud microphysics and radiative forcing (Dai, 2006). Amongst these processes, cumulus convection plays a particularly important role in regulating the pattern and temporal variation in precipitation in RCMs, especially in summer. Many studies have documented that the simulation of precipitation by RCMs is sensitive to the choice of the cumulus schemes. For example, Giorgi and Shields (1999) tested a series of cumulus schemes at a resolvable scale within a collection of RCMs to conclude that the simplified explicit moisture and Grell schemes capture the precipitation best at both a regional spatial scale, and monthly to seasonal temporal scale, throughout the United States. Using the MM5 model, Gochis et al. (2002) showed the superiority of the Kain–Fritsch cumulus scheme over the Betts–Miller–Janjić, Grell and Kuo schemes in representing the precipitation during the North American monsoon in 1999. However, Xu and Small (2002) argued that the Grell scheme performs better than Kain–Fritsch scheme in depicting the intraseasonal and interannual variations in North American monsoon (NAM) rainfall. Liang et al. (2004)

*Corresponding author. e-mail: shibogao@126.com

Citation: Tellus A: 2017, **69**, 1406264, https://doi.org/10.1080/16000870.2017.1406264

demonstrated that Kain–Fritsch cumulus scheme is superior in reducing the summer precipitation bias in the NAM region and along the East Coast of the United States, but the Grell scheme has more advantages in representing the rainfall in Midwest and Atlantic Ocean. Recently, similar intercomparison studies have been conducted on the effectiveness of cumulus schemes for simulating precipitation, including the summer mean pattern, annual and diurnal cycles, interannual variation and the frequency of precipitation on a daily time scale (Ratnam and Kumar, 2005; Qiao and Liang, 2014; Ratna et al., 2014).

Although many numerous cumulus schemes have been developed, each has its own advantages and disadvantages, depending highly on the weather and climate patterns. An optimal ensemble of multiple cumulus schemes has been developed by Liang et al. (2007) to combine the superiority of different cumulus schemes for the improvement of the skill of precipitation forecasting, whereby an ensemble of two members using different cumulus schemes are generated and the optimal weight is calculated by minimizing the root mean square errors (RMSE) and maximizing the temporal correlations with observations. Liang et al. (2007) demonstrated that both the interannual variability and climate mean of the summer precipitation over the United States and Mexico are improved significantly by the optimal weight ensemble, compared with the member using only the Kain–Fritsch or Grell schemes.

The precipitation features over China are mainly controlled by the East Asian monsoonal system, where the rainfall in the summer season accounts for the majority of the total annual precipitation. RCM simulations show a large variability, with the uncertainty of monsoonal precipitation related to deficiencies in the performance of the cumulus scheme. Lee et al. (2005) found that Anthes-Kuo and Grell schemes more realistically reproduced the summer flood in 1998 than the Kain–Fritsch scheme over China. Yu et al. (2011) showed that Grell scheme performed better than Kain–Fritsch and Betts–Miller–Janjić schemes in simulating the overall summer monsoon precipitation over China. Liu et al. (2009) investigated four different cumulus schemes over China using the Regional Climate Model Version 3, and found the ensemble always produces a smaller bias in precipitation than the individual schemes in both 1991 and 1998. As this study was only carried out for the summer of 1991 and 1998, more work is needed to be able to evaluate the performance for long-term simulations.

Our aim is to investigate the impact of different cumulus schemes on the simulation of precipitation over China for the period 1982–2004 using the Weather Research and Forecasting (WRF) model. To quantify the possible causes of any deficiency in downscaling by the WRF model, we adopt reanalysis data as the forcing data, since it is considered to provide 'perfect' lateral boundary conditions (Chen et al., 2016). We first compared the performance of the Kain–Fritsch and Grell cumulus schemes, after which the optimal ensemble approach obtained the optimal localized weights of these two cumulus schemes. This approach shows some improvements over the other two schemes in terms of precipitation over China.

In this paper, the model design, observational data used for model verification and the method of optimal ensemble weighting from these cumulus schemes is present in Section 2. The WRF downscaling results for the two cumulus schemes, and the results of the optimal ensemble approach is given in Section 3. The results and conclusions are summarized in the final Section.

2. Model, data and methodology

2.1. *Experiment design and observation*

The RCM used is the WRF-ARW (Advanced Research WRF) model version 3.4.1 (Skamarock et al., 2008) developed at the National Center for Atmospheric Research (NCAR). The initial and lateral boundary conditions for the WRF model are sourced from the National Centers for Environmental Prediction-Department of Energy (NCEP-DOE) global reanalysis (Reanalysis II; Kanamitsu et al., 2002) and updated at 6-h intervals. The sea surface temperature (SST) is obtained from the daily National Oceanic and Atmospheric Administration (NOAA) optimum Interpolation SST (OISST; Reynolds et al., 2002) data-set. Both the Reanalysis II data and SST have a resolution of 2.5° × 2.5°.

The model domain centred at (35.17°N, 110°E) covers the whole of China using the Lambert conformal map projection (see Fig. 1). The horizontal grid resolution is 30 km, with 231 × 171 horizontal grid points and 37 vertical levels extending up to 50 hPa. The vertical resolution is about 550 m. The buffer zones are located along the four domain edges with widths of 14 grid points as that of Chen et al., (2016), where the dynamic relaxation technique (Davies and Turner, 1977) is used to avoid sharp gradients resulting from the difference between reanalysis data and the inner WRF simulation domain. Figure 1 includes the geographic terrain height over China, which generally increases from east to west. The Tibetan Plateau is found to the west with the highest mountains extending to 5500 m, and various mountain chains within the northern and central regions with heights ranging from 500 to 3000 m. Eastern China is marked with plains and hills with heights less than 500 m. The borders in Fig. 1 demarcate seven sub-regions with different climate characteristics, including Northeast China (NE), North China (NC), the Yangtze River (YZ), Southeast China (SE), Northwest China (NW), the Tibetan Plateau (TB) and Southwest China (SW), for which detailed modelling results will be presented below.

The physical parameterizations chosen include the WRF Single-Moment 6-class (WSM6) microphysical scheme (Hong and Lim, 2006), Dudhia shortwave radiation (Dudhia, 1989), the Rapid Radiative Transfer Model (RRTM) longwave

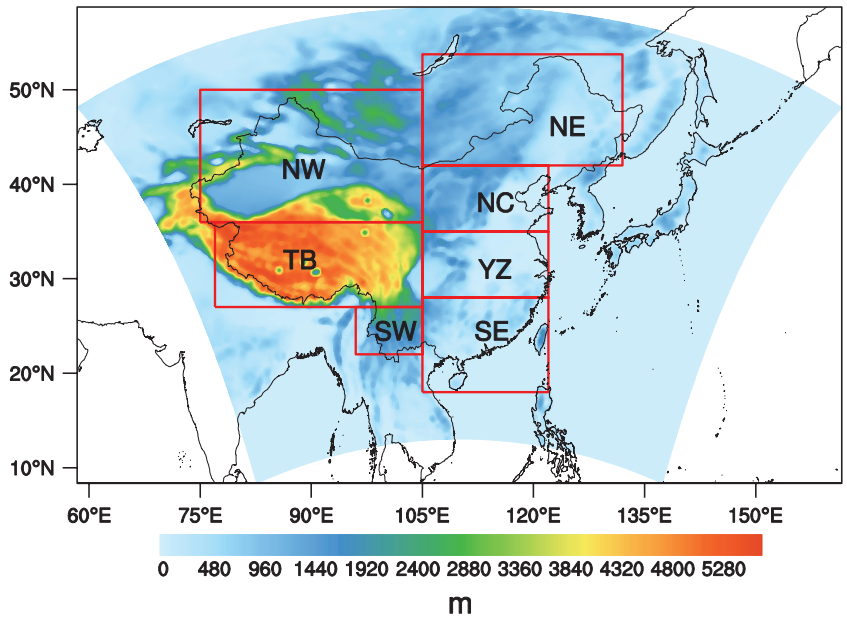

Fig. 1. Model domain and topography (units: m) over china. Boxes represent the selected regions: Northeast China (NE), North China (NC), Yangtze River (YZ), Southeast China (SE), Northwest China (NW), Tibetan Plateau (TB) and Southwest China (SW).

radiation (Mlawer et al., 1997), Yonsei University (YSU) planetary boundary-layer scheme (Noh et al., 2003), and the Noah land surface model (Chen and Dudhia, 2001). Two experiments were integrated continuously during 1982–2004 because both the OISST and Reanalysis II data are available for this period. The first month is regarded as a spin-up period and not accounted in the analysis. These two experiments differ in their use of the Kain–Fritsch (Kain, 2004) and Grell cumulus (Grell, 1993) schemes for studying the sensitivity of the summer precipitation to the cumulus schemes.

To validate the results of the dynamical downscaling, we use daily surface air temperature and precipitation data from a high-quality daily gridded CN05.1 data-set, which has a resolution of 0.25° × 0.25°. It was generated by interpolating 2400 observation stations from the China Meteorological Administration using the anomaly approach (Xu et al., 2009). The anomaly approach first calculates a gridded climatology, then the final data-set is obtained by adding a gridded daily anomaly to the climatology. These data have been shown to be reliable and widely used in the evaluation of model performance over China (Yu et al., 2011; Bao et al., 2015; Yu et al., 2015; Yang et al., 2016). The CN05.1 data-set is interpolated to the WRF grids using the objective analysis interpolation (Barnes, 1964).

2.2. *Extreme precipitation indices*

As used in previous studies (Zhang et al., 2011; Li et al., 2013; Jiang et al., 2015), three common extreme precipitation indices calculated from daily data were selected for studying extreme precipitation (Table 1). The simple daily intensity index (SDII) describes the mean rainfall amounts of daily precipitation larger than 1 mm, and the annual account of days with daily precipitation greater than 10 mm (R10) represents the frequency of heavy precipitation. The R95p index refers to the annual precipitation amount of the daily precipitation greater than 95th percentile of wet days, which describes very extreme precipitation based on the threshold.

Table 1. Indicator, acronym and definition of three precipitation extreme indices used in the study.

Indicator	Acronym	Definition	Units
Simple daily intensity	SDII	Annual precipitation amount on wet days (daily precipitation larger than 1 mm)	mm/day
Heavy precipitation days	R10	Number of days with daily precipitation above 10 mm	days
Extreme precipitation amount	R95p	Annual precipitation amounts of daily precipitation above the 95th percentile of wet days	mm

2.3. *Ensemble optimization solution*

The optimal ensemble solution is assumed to be a linear combination of the two cumulus schemes, which is defined following Liang et al. (2007) as

$$P_{\mathrm{ENS}}(s,\alpha,t) = \alpha(s)P_{\mathrm{GR}}(s,t) + [1-\alpha(s)]P_{\mathrm{KF}}(s,t), \quad (1)$$

for

$$0 \le \alpha \le 1, \quad (2)$$

where $P_{ENS}(s, \alpha, t)$ is the variable to be estimated, here denoting the daily precipitation. The variables in the parentheses are the dependent variables, with s for space and t for time, α is the optimal weighting to be determined and is a function of s. Here, $P_{GR}(s, t)$ and $P_{KF}(s, t)$ represent the WRF simulated precipitation based on the Grell and Kain–Fritsch cumulus schemes.

The main goal is to find the optimal weight assigned between the Kain–Fritsch and Grell schemes for each WRF grid point for determining the model forecast variables that represent the observations most accurately. A feasible sequential quadratic programming algorithm is an effective method for minimizing a set of smooth objective functions, which are constrained by equality and inequality equations, are linear and nonlinear, and have constant bounds on the variables (Zhou et al., 1997). An objective function $F(s, \alpha)$ also needs to be designed prior to the performing of the minimization procedure within the optimization solver in estimating

$$F(s, \alpha) = \text{RMSE}\,(s, \alpha)(1 - \text{COR}\,(s, \alpha)), \tag{3}$$

where

$$\text{RMSE}\,(s, \alpha) = \frac{1}{N}\sqrt{\sum_{t=1}^{N}\left(P_{ENS}(s, \alpha, t) - P_{OBS}(s, t)\right)^2} \tag{4}$$

and

$$\text{COR}\,(s, \alpha) = \frac{\sum_{t=1}^{N}\left(P_{ENS}(s, \alpha, t) - \overline{P_{ENS}(s, \alpha, t)}\right)\left(P_{OBS}(s, t) - \overline{P_{OBS}(s, t)}\right)}{\sqrt{\sum_{t=1}^{N}\left(P_{ENS}(s, \alpha, t) - \overline{P_{ENS}(s, \alpha, t)}\right)^2}\sqrt{\sum_{t=1}^{N}\left(P_{OBS}(s, t) - \overline{P_{OBS}(s, t)}\right)^2}}. \tag{5}$$

Here, RMSE(s, α) and COR(s, α) are the root mean square error and correlation coefficient between the variables simulated by the WRF model with Kain–Fritsch or Grell scheme, and the observations $P_{OBS}(s, t)$ at each gird cell, where 23 years (1982–2004) of daily precipitation data during summer are used to train the optimizing weight, N is total number of daily data, and the overbar ($\bar{}$) represents a temporal mean.

3. Results

3.1. Precipitation of individual cumulus schemes

Figure 2 compares the geographic distribution of the observed 1982–2004 winter (DJF), summer (JJA) and annual (ANN) mean precipitation, with WRF simulations using the Kain–Fritsch and Grell cumulus schemes. In winter, the observed precipitation decreases from the southeast to the northwest, with a maximum value of 3 mm (Fig. 2a). Both the Kain–Fritsch and Grell schemes exhibit similar patterns, but with a dry bias over the southeast region and a wet bias over northwest and west regions, respectively. Although both schemes underestimate the precipitation in southeast, it is clear that the Kain–Frisch scheme produces an overall more realistic spatial pattern than the Grell scheme. As shown in Fig. 2b, precipitation reaches its peak with the largest areal coverage during summer, which is associated with the typical East Asian monsoonal period, and appears as two major rainbands. One rainband is located in southern China and the other in the Yangtze River basin, with the maximum value of 12 mm. These two rainbands are generally overestimated by Kain–Fritsch scheme, while underestimated by Grell scheme. The observed annual mean precipitation shows similar distribution patterns as in winter, but with greater values. The precipitation amounts are also relatively high in southern China and Yangtze River (wet region), and low in northern China and Tibetan Plateau (dry region). The Kain–Fritsch scheme produces excessive rainfall in the Yangtze River basin, but with a dry bias of 2 mm in southeastern China, while the Grell scheme once more generates weaker precipitation over these regions.

Figure 3 presents the annual cycle of precipitation according to the observations and WRF simulations with Kain–Fritsch and Grell schemes over the seven sub-regions (Fig. 1). The seasonal cycle in the dry regions (NE, NC, NW and TB) is generally better captured by the Grell scheme, and the wet regions (SE, SW and YZ) is better captured by the Kain–Fritsch scheme, with the exception of the Yangtze River region. For example, for the northeast and northern regions, the Grell scheme reduces the wet bias by about 40 and 45% from KF scheme, respectively. In the Tibetan Plateau region, both schemes overestimate the precipitation by 30–80% in the cold season (from October to April), but the Grell scheme matches better with observations than the Kain–Fritsch scheme in summer. In the northwestern region, both schemes produce a wet bias in the cold season and a dry bias in summer, but Grell scheme reduces the wet bias by 3% from KF scheme. In the Yangtze River region, the Kain–Fritsch scheme overestimates the precipitation from April to September by 10–25%, while Grell scheme underpredicts by 9–15% with an excellent match with observations from April to June. However, Kain–Fritsch scheme is better in predicting the annual cycle phase than the Grell scheme with higher correlation coefficients (0.996, 0.971, see Fig. 3). The Kain–Fritsch scheme has the most realistic simulation over the rainy southeast region, with a significant improvement over the Grell scheme from May to September. In the southwest region, the observed peak precipitation in both experiments shows a phase shift; however, the Kain–Fritsch scheme produces more realistic rainfall in terms of magnitude. The Grell scheme is close to the Kain–Fritsch scheme from January to April, but a substantial underestimation by 38–75% is found in the following month. Both schemes cannot well represent the annual cycle

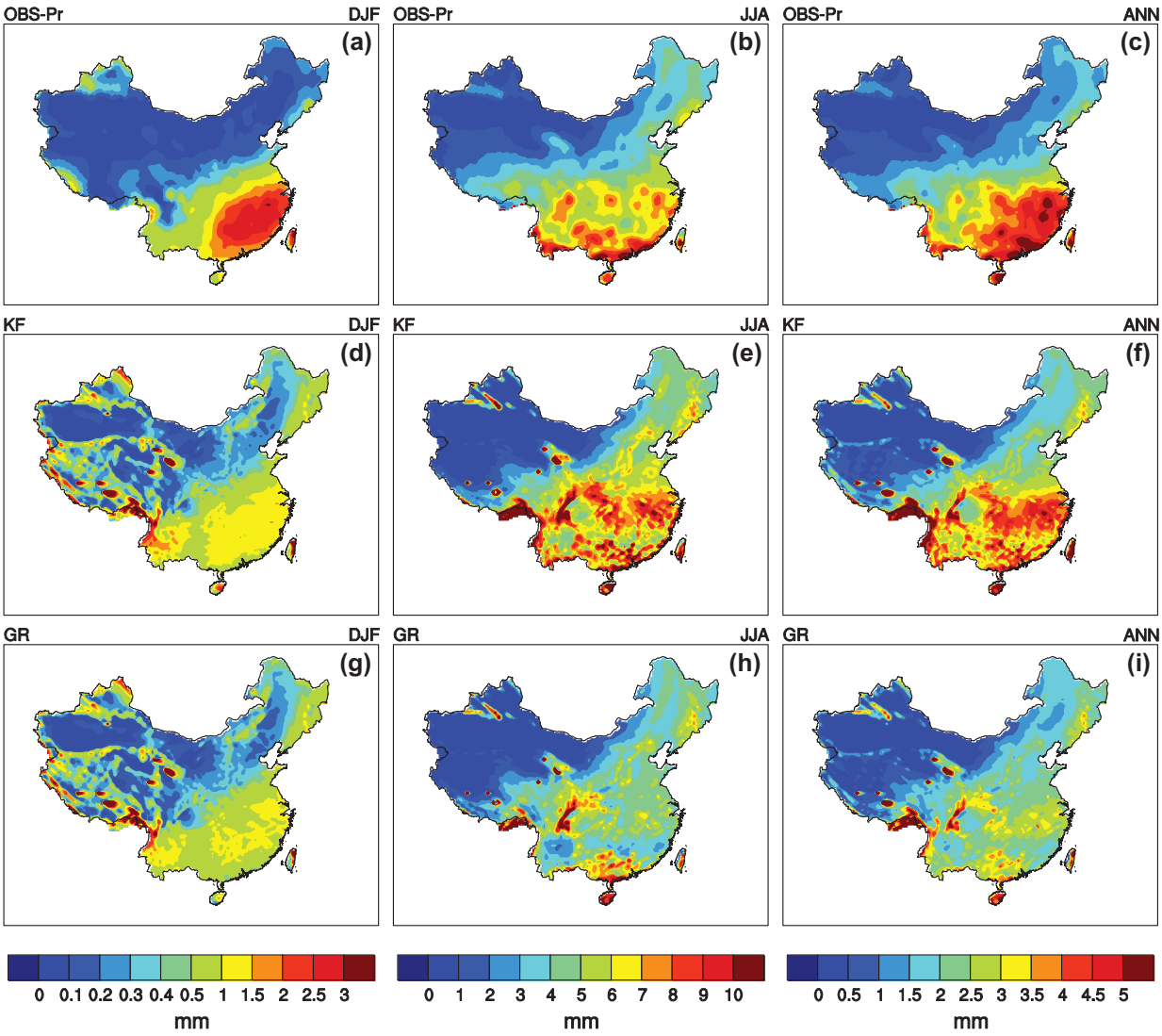

Fig. 2. Spatial distributions of seasonal mean (DJF (a, d, g), JJA (b, e, h), ANN (c, f, i)) precipitation (units: mm) during 1982–2004 from observation (a–c), WRF model with Kain–Fritsch (d–f) and Grell (g–i) cumulus schemes. Note that the colourbar scales are different.

phase over southwest, northwest and Tibetan Plateau regions, which may be attributed to the topographic effect (Duan et al., 2012).

Figure 4 compares the observed and simulated interannual anomalies of area-averaged summer precipitation for the seven sub-regions over China. Amongst these regions, the southeast region produces the largest interannual variations, ranging from −0.8 to 1.2 mm. Both schemes simulate the interannual variations in the northwest region well, with correlation coefficients above 0.84. The region with the worst simulated interannual variations for the two schemes is the Tibetan Plateau region, where the Grell scheme produces a relatively higher correlation of 0.424 compared with the Kain–Fritsch scheme. For the Yangtze River and southwest regions, the correlation coefficients with observations for the Kain–Fritsch scheme is 0.547 and 0.523, respectively, and 0.487 and 0.435 for the Grell scheme, respectively. For the other regions, including the northeast, northern, northwest, southeast and Tibetan Plateau regions, the Grell scheme has higher correlation coefficients than the Kain–Fritsch scheme.

Figure 5 shows Taylor diagrams that compare summer precipitation simulated by the Kain–Fritsch and Grell schemes with respect to the observations. The Taylor diagrams statistically summarize the differences between simulations and observations according to the correlation coefficient, RMSE and the ratio of variances between the models and observations (Taylor, 2001). The reference (REF) point indicates a perfect simulation, in which the spatial correlation and ratio of the spatial standard deviations are equal to 1, and the centred pattern RMS error (RMSE) is equal to 0. For the northeast, northwest

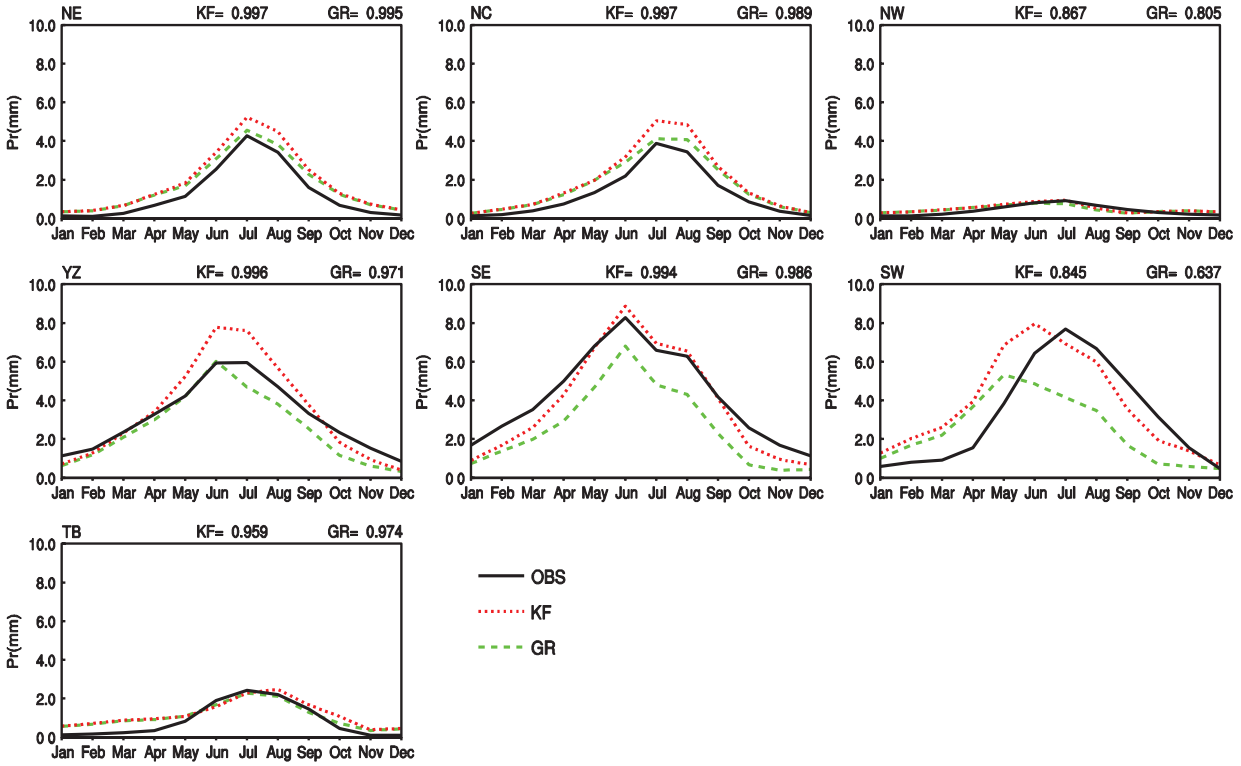

Fig. 3. Annual cycle of precipitation (units: mm) over sub-regions during 1982–2004 from observation (solid black line), and WRF model with Kain–Fritsch (dotted red line) and Grell cumulus (dashed green line) schemes. The annual cycle correlation coefficients of the result of Kain–Fritsch and Grell cumulus schemes with observation are labelled at the top of each panel.

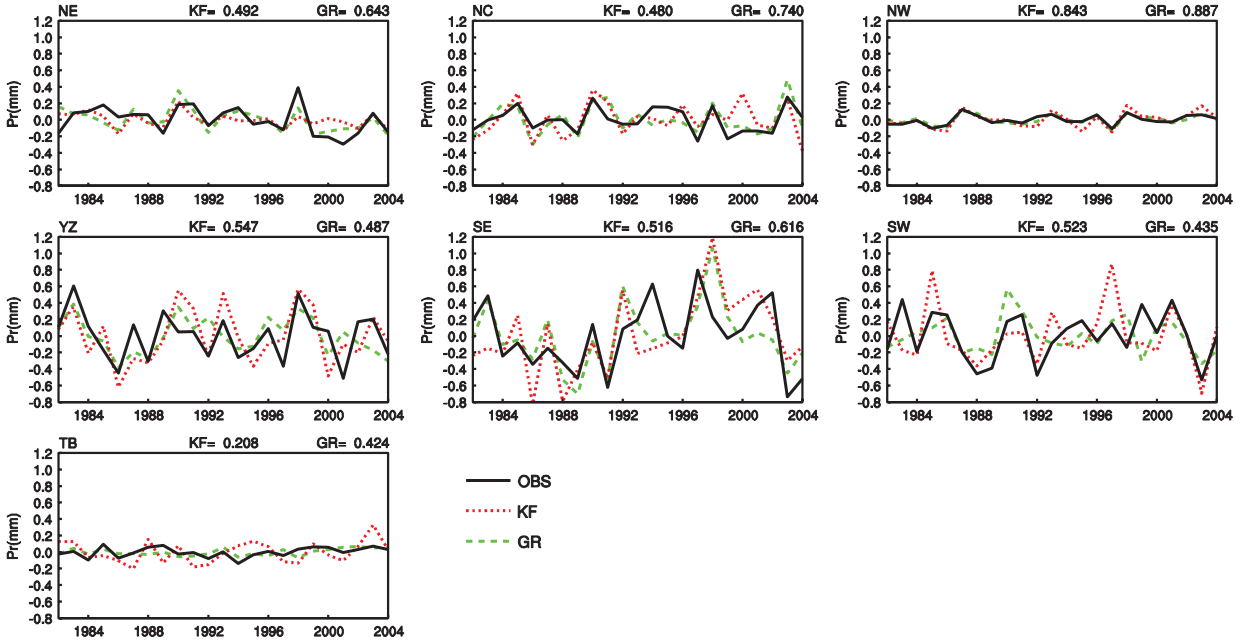

Fig. 4. Interannual anomalies of area averaged summer precipitation (units: mm) over sub-regions during 1982–2004 from observation (solid black line), and WRF model with Kain–Fritsch (dotted red line) and Grell cumulus (dashed green line) schemes. The interannual correlation coefficients of the result of Kain–Fritsch and Grell cumulus schemes with observation are labelled at the top of each panel.

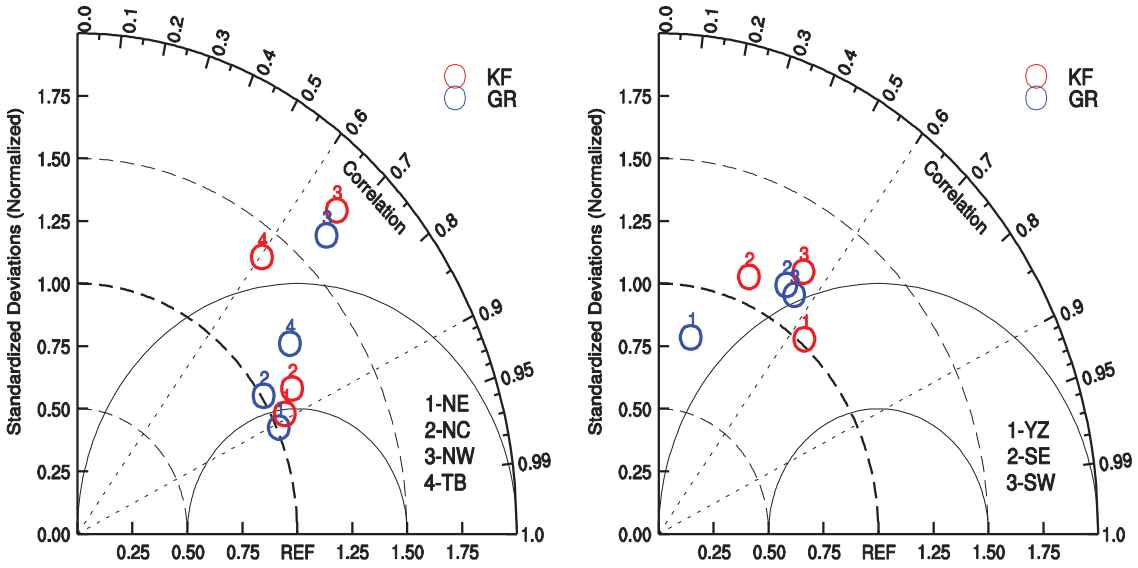

Fig. 5. Taylor diagrams for the summer mean precipitation over dry (left panel) and wet (right panel) regions from WRF model with Kain–Fritsch (red circles) and Grell (blue circles) cumulus schemes.

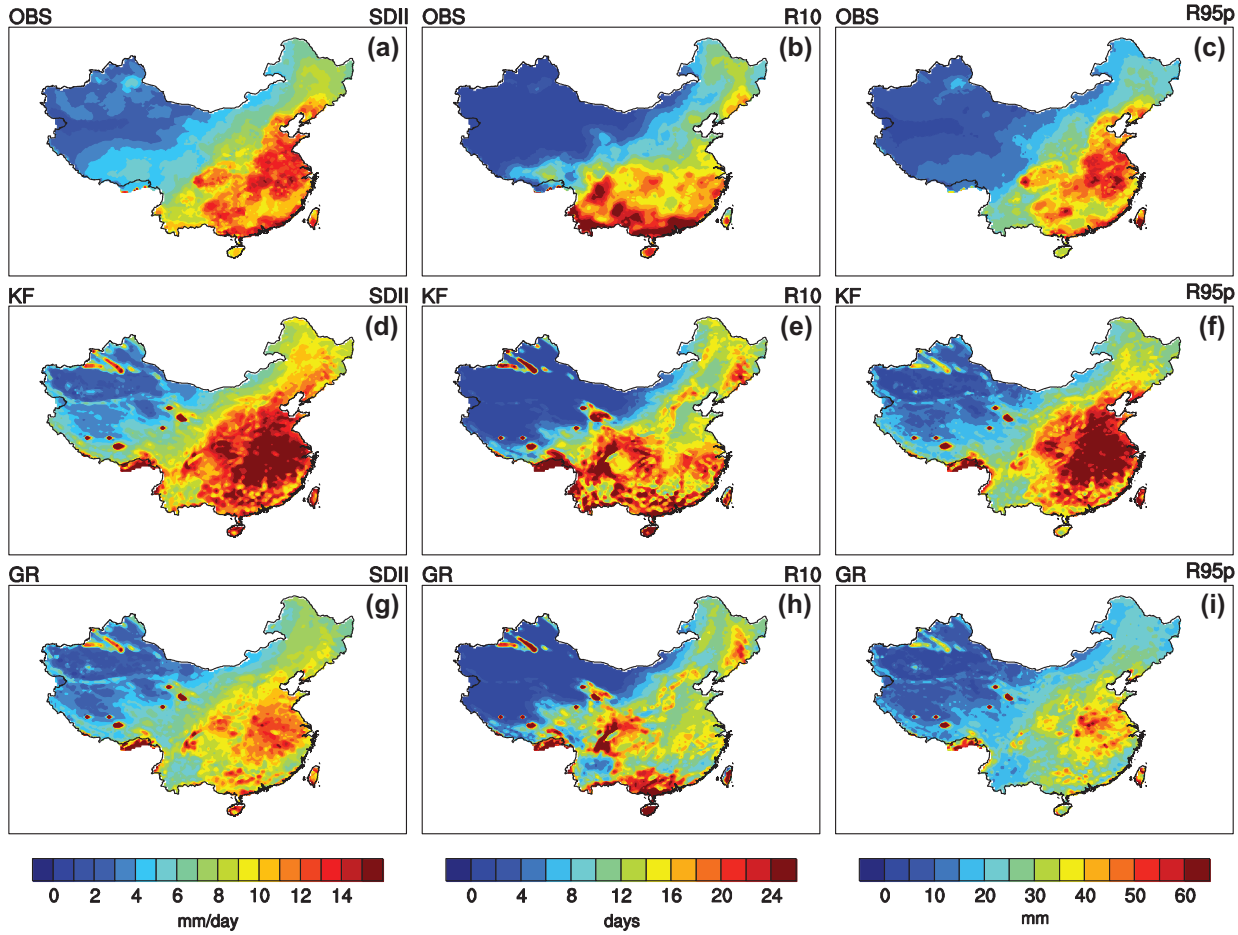

Fig. 6. Spatial distributions of summer extreme precipitation indices (SDII (a, d, g), units: mm/day; R10 (b, e, h), units: days; R95p (c, f, i), units: mm) from observation (a–c), WRF model with Kain–Fritsch (d–f) and Grell (g–i) schemes. Note that the colourbar scales are different.

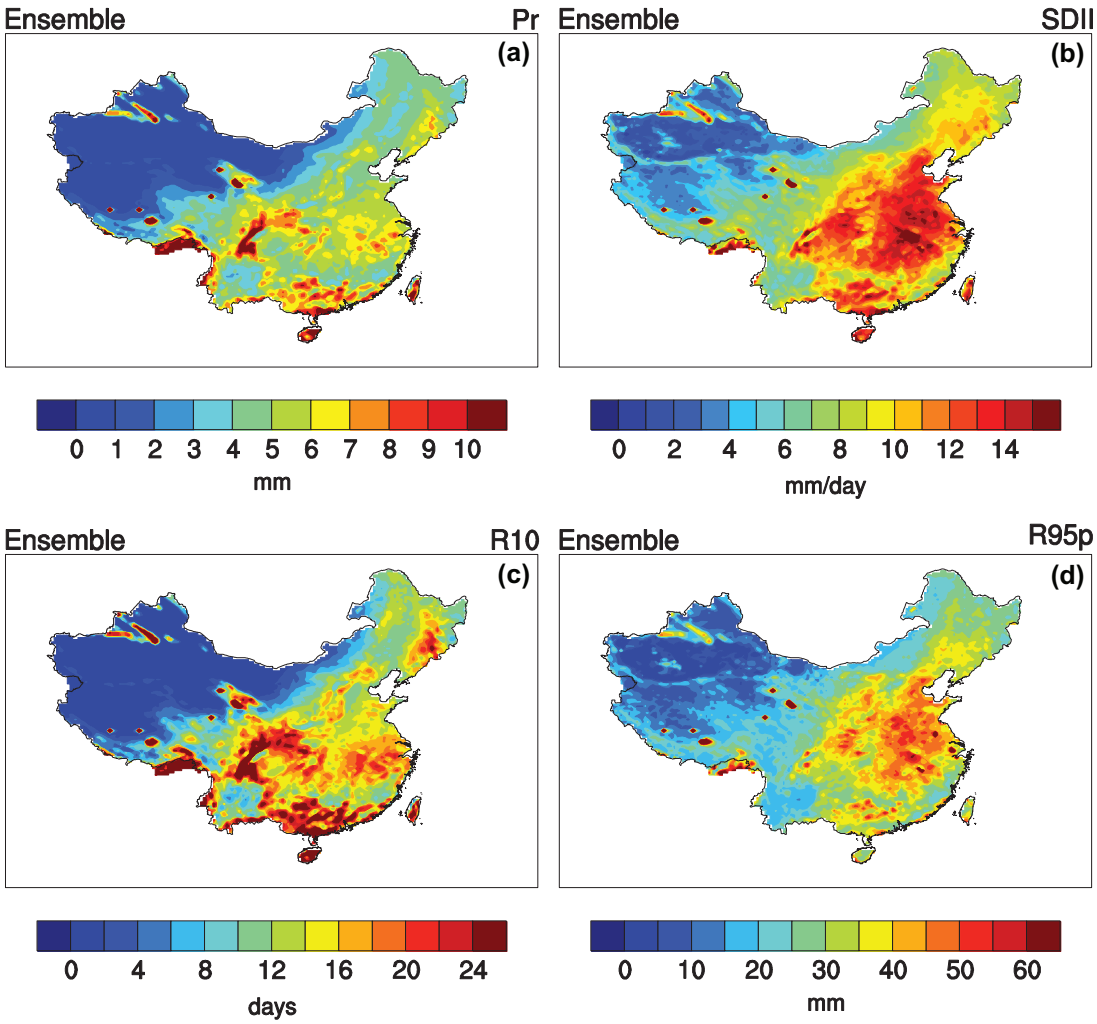

Fig. 7. Spatial distributions of ensemble summer mean precipitation (a), (Pr, units: mm) and extreme precipitation indices (b–d) (SDII (b), units: mm/day; R10 (c), units: days; R95p (d), units: mm). Note that the colourbar scales are different.

Table 2. RMSE of summer precipitation and extreme precipitation indices between Kain–Fritsch, Grell, Ensemble and observation.

	KF	GR	Ensemble
Pr	3.42	3.48	**3.40**
SDII	3.39	2.89	**2.73**
R10	6.35	6.29	**6.01**
R95p	14.54	11.39	**10.48**

Note: Figures in bold indicate improvement (lower RMSE) compared to KF and GR.

and Tibetan Plateau regions, the precipitation is better simulated by the Grell scheme, with higher correlation coefficients and lower RMSE. For the northern region, differences in the RMSE and correlation coefficient between the two schemes is not obvious, but the normalized standard deviation between the Grell scheme and observations is closer to one. The Grell scheme performs quite poorly in the Yangtze River region with a correlation coefficient of 0.3, but is improved by the Kain–Fritsch scheme with a higher correlation coefficient of 0.7. The RMSE is also reduced by Kain–Fritsch scheme from 1.1 to 0.75. For the southwest region, the Kain–Fritsch scheme improves the correlation coefficient from 0.45 to 0.58 over the Grell scheme, with the normalized standard deviation being closer to one. For the southeast region, the two schemes provide similar spatial variances, but with the correlation coefficient of the Grell scheme relatively higher than the Kain–Fritsch scheme.

To further evaluate extreme precipitation characteristics, Fig. 6 compares the distribution of the 1982–2004 summer mean extreme precipitation indices, including SDII, R10 and R95p over China with observations, and WRF simulation with the Kain–Fritsch and Grell schemes. The largest values of SDII in observation are mainly found in the Yangtze River basin, over Southeast China and in the Sichuan basin (Fig. 6a). A significant overestimation with the maximum value

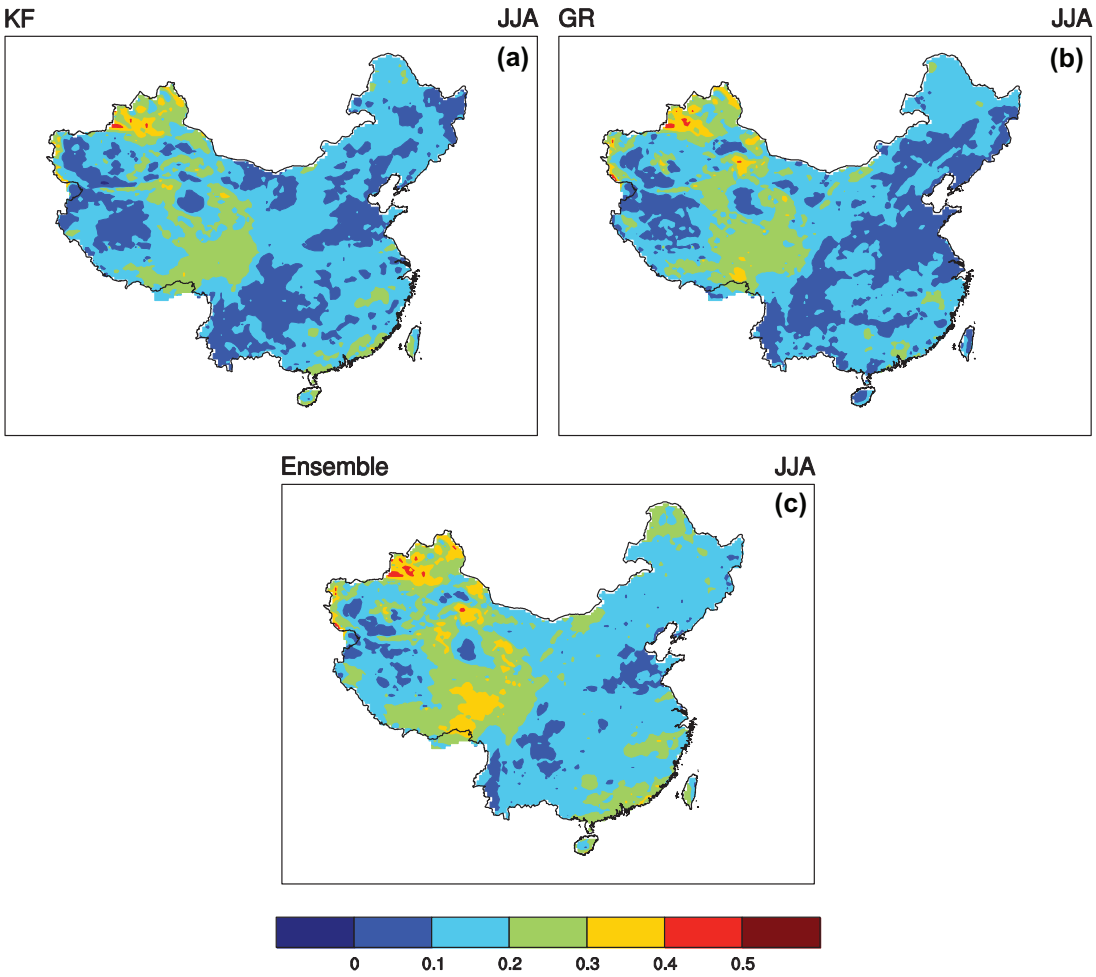

Fig. 8. Spatial distributions of 1982–2004 temporal correlation coefficient of summer mean precipitation for WRF model with Kain–Fritsch (a), Grell cumulus schemes (b) and their ensemble result (c).

of 18 mm over these regions is apparent in the Kain–Fritsch scheme (Fig. 6d). The Grell scheme produces, in general, a smaller bias than the Kain–Fritsch scheme, with a tendency to underestimate the SDII over the Yangtze River basin and northeast China (Fig. 6g). As shown in Fig. 6b, observations in the southeast and southwest regions of China reveal a high frequency of heavy precipitation (R10), with the maximum value of 25 days. The high R10 over the southeast coast is simulated well by the two schemes, but the amount and distribution are better captured by Kain–Fritsch scheme. However, the Kain–Fritsch scheme produces a more realistic magnitude of precipitation in the southwest region than the Grell scheme (Fig. 6e). A further anomalously large value of R10 as found over the Yangtze River basin is overestimated by the Kain–Fritsch scheme, but underestimated by the Grell scheme. The R95p index according to the observations has similar distribution patterns with the SDII index (Fig. 6c). The Grell scheme captures the locations of the larger values, but with insufficient amounts, while the Kain–Fritsch scheme overestimates the amount by 18 mm and with a much wider coverage that extended to southeastern China. It is also found that the large value of R95p over the southern coast is poorly simulated by the two cumulus schemes.

The above analyses show that the Kain–Fritsch and Grell schemes have distinctive skills in the simulation of the summer precipitation characteristics, with a strong regional dependence. Because of the large uncertainty in the WRF simulation depending on the cumulus scheme used, it is necessary to use an optimal ensemble technique to improve the WRF downscaling skill of summer rainfall over China.

3.2. *Optimal ensemble results*

The ensemble summer mean precipitation as well as three extreme precipitation indices based on the optimal weight are illustrated in Fig. 7, where it is clear that the ensemble is superior to both the Kain–Fritsch and Grell schemes in most of the regions for the summer mean precipitation. As shown in

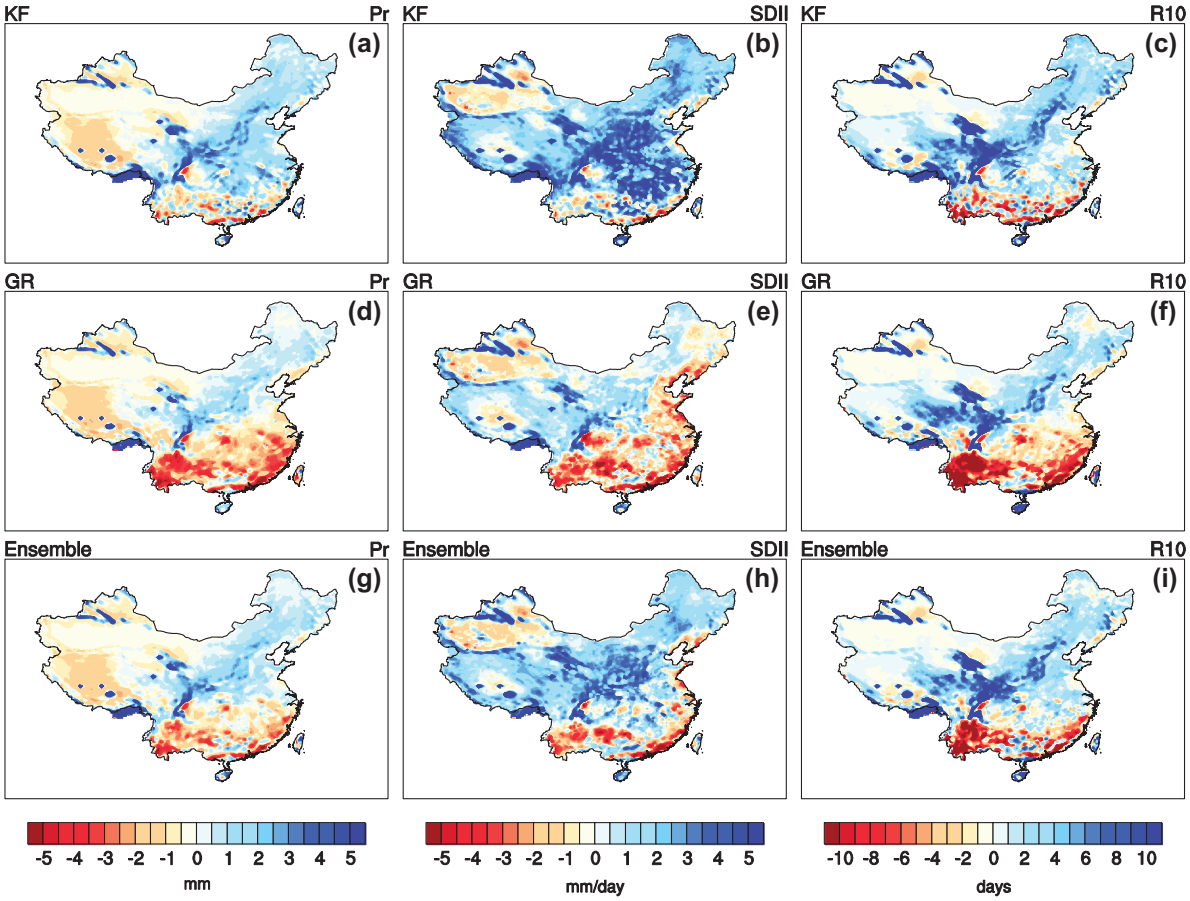

Fig. 9. Spatial distributions of 1982–2004 biases of summer mean precipitation (a, d, g) (Pr, units: mm) and extreme precipitation indices (b, c, e, f, h, i) (SDII (b, e, h), units: mm/day; R10 (c, f, i), units: days) from WRF model with Kain–Fritsch (a–c), Grell (d–f) cumulus schemes and their ensemble result (g–i). Note that red colours represent a dry bias and blue colours represent a wet bias and the colourbar scales are different.

Fig. 2(e, f), over the Yangtze River basin and southern China, the Kain–Fritsch scheme yields excessive rainfall, but is underestimated by the Grell scheme. In contrast, the ensemble generates a substantially improved precipitation amount and pattern over these regions, as well as a more realistic magnitude over southern and northeast China (Fig. 7a). The overestimation by the Kain–Fritsch scheme and the underestimation by the Grell scheme are more evident for the three extreme indices, especially for SDII and R95p. The ensemble shows some advantages over the individual schemes, with the magnitude falling between the Kain–Fritsch and Grell schemes (Fig. 7b, d). However, some spurious precipitation in northwest and Tibetan Plateau also exist in the ensemble, which are carried from its individual member scheme.

To assess their performances quantitatively, the RMSE of summer precipitation and extreme indices between the three datasets and observations over continental China are listed in Table 2. For the summer mean precipitation, the RMSE decreases from 3.42 to 3.48 for the Kain–Fritsch and Grell schemes, respectively, to 3.40 for the ensemble approach. For the extreme indices, the ensemble approach has the lowest RMSE, followed by the Grell scheme. The ensemble reduces the RMSE by 19, 5 and 28% with respect to the Kain–Fritsch scheme for the SDII, R10 and R95p indices.

Figure 8 shows the distribution of temporal correlation coefficient of summer mean precipitation for the Kain–Fritsch and Grell schemes and the ensemble of 1982–2004. The ensemble shows the highest correlation coefficients along the southern Tibetan Plateau and northwestern China with the maximum value of 0.5, followed by the Grell scheme. The ensemble approach also performs better than the two schemes, with a larger area of correlation coefficient above 0.2 in Southwest China and the Yangtze River basin, with the Grell scheme producing the lowest correlation coefficient over these regions (Fig. 8b). The correlation coefficient of the ensemble is also relatively better than the two schemes in Northwestern China, which is increased by 10 and 15% for Kain–Fritsch and Grell scheme, respectively. On average, the correlation coefficient of the

ensemble is larger than 0.1 in most regions, confirming the accuracy of the optimized method.

To further highlight the regional differences of the Kain–Fritsch and Grell schemes and the ensemble approach, the bias for the summer mean precipitation and extreme precipitation indices are presented in Fig. 9. For the precipitation, the Kain–Fritsch scheme mainly shows a wet bias ranging from 2 to 4 mm, which is mainly located in the Yangtze River basin and Northeastern China (Fig. 9a), while the Grell scheme produces a systematic dry bias of 2–5 mm over Southern China (Fig. 9d). However, these biases tend to become smaller in the ensemble approach, suggesting its advantage over the two schemes alone in producing the summer mean pattern and amount. For the SDII index, the Kain–Fritsch scheme produces a large wet bias of approximately 3–5 mm over the Northern China and Yangtze River regions (Fig. 9b), which is improved by the Grell scheme by more than 1–2 mm (Fig. 9e). In the rainy regions, the Grell scheme generally produces a dry bias, with the maximum value along the southern coast and Southeast China. The ensemble approach corrects some bias from both schemes, especially in Northern China for the Kain–Fritsch scheme and Southwest China for Grell scheme (Fig. 9h). For the R10 index, the ensemble reveals a smaller area of wet bias above 4 mm than the Kain–Fritsch scheme in the northern China region, which is also true for the Grell scheme, but with a large dry bias of 6–8 mm in the Southwest China and southeast coastal regions, while it is reduced by the ensemble approach by 2–4 mm over these regions (Fig. 9i). For the R95p index, the two schemes show a similar pattern as SDII, but with larger biases exceeding 18 mm (Figure not shown). The ensemble also showed better skill than the individual schemes by reducing the wet bias for the Kain–Fritsch scheme over the Yangtze River region and the dry bias for the Grell scheme over Southern China (Figure not shown). However, the ensemble is not always the best in the simulation of precipitation and extreme precipitation, such as the larger bias than KF scheme along the southern coast (Fig. 9c, f, i).

4. Summary and conclusion

In this paper, the impact of the Kain–Fritsch and Grell cumulus schemes on the simulation of precipitation is investigated through long-term simulations with the WRF model driven by NCEP Reanalysis II data at a 30-km horizontal resolution during the period of 1982–2004. The model performance is evaluated by comparing the simulations with observations from the CN05.1 data-set.

The results indicate that while the Kain–Fritsch and Grell schemes capture the location of rain belts, they have distinctive skills in the simulation of the precipitation amount and pattern, with a strong regional dependence. While the precipitation is underestimated by both schemes in winter, the Kain–Fritsch scheme improves the simulation of the amount of precipitation in southeastern China, but tends to overestimate the summer and annual mean precipitation in the Yangtze River basin, and Southern and Northeastern China regions, which are underestimated by the Grell scheme. The WRF downscaling skill reduction in winter for precipitation may be associated with model deficiencies in representing the snow feedback processes (Hall and Qu, 2006).

For the annual cycle of regional mean precipitation, the Grell scheme produces lower correlations with observations than the Kain–Fritsch scheme in most regions, but reduces the wet bias in the Northwest, Northern China and Tibetan Plateau regions. In the wet regions, including Southeast and Southwest China, the Kain–Fritsch scheme performs better than the Grell scheme with a higher correlation and smaller bias. The precipitation in the Yangtze River basin is better captured by the Kain–Fritsch scheme with higher correlation, but overestimates the precipitation in summer. These features are also confirmed by normalized Taylor diagrams. The interannual variation in summer precipitation is better represented by the Grell scheme in most of the regions except for the Yangtze River basin and Southwest China.

For the simulation of extreme precipitation, the two schemes are able to capture the observed features, but the overestimation by the Kain–Fritsch scheme in the Yangtze River basin, Northern and Northeast China, and underestimation by the Grell scheme over Southern China is evident, especially for the SDII and R95p indices. However, the Grell scheme exhibits a lower RMSE with respect to the observations than the Kain–Fritsch scheme.

The ensemble method based on the outcomes of the Kain–Fritsch and Grell schemes, whose relative weighs are optimized to yield overall mimimum of the objective function of RMSE(1 − COR) with respect to the observed daily precipitation during summer, performs better than the individual schemes for precipitation as well as extreme precipitation, with the magnitude falling between the Kain–Fritsch and Grell schemes. The RMSE is lower than the Kain–Fritsch and Grell schemes for both precipitation and extreme precipitation, while also producing a lower temporal correlation over all of China, especially in the southern Tibetan Plateau, Northwestern China, Southwest China and Yangtze River basin. Note that this ensemble method can minimize the bias from the Kain–Fritsch or Grell schemes. However, the ensemble cannot eliminate the biases which simulated by both of the two schemes. The bias of the ensemble is between the Kain–Fritsch and Grell schemes over the region where a large deficit exists. Therefore, further studies are necessary to improve the ensemble performance for other solutions to optimize the weights, or use more cumulus schemes to minimize the bias. Subgrid-scale cloud-radiation interactions within the KF scheme have also been found to be important (Alapaty et al., 2012; Herwehe et al., 2014) in the simulation of precipitation, and thus should be explored in future studies.

Disclosure statement

No potential conflict of interest was reported by the authors.

Funding

This work was supported by the Research Innovation Program for College Graduates of Jiangsu Province [grant number KYLX_0829] and [grant number KYLX_0844]. Authors Shibo Gao and Danlian Huang are supported by the scholarship from the China Scholarship Council.

References

Alapaty, K., Herwehe, J. A., Otte, T. L., Nolte, C. G., Bullock, O. R. and co-authors. 2012. Introducing subgrid-scale cloud feedbacks to radiation for regional meteorological and climate modeling. *Geophys. Res. Lett.* **39**, L24809.

Bao, J., Feng, J. and Wang, Y. 2015. Dynamical downscaling simulation and future projection of precipitation over China. *J. Geophys. Res. Atmos.* **120**, 8227–8243.

Barnes, S. L. 1964. A technique for maximizing details in numerical weather map analysis. *J. Appl. Meteorol.* **3**, 396–409.

Chen, F. and Dudhia, J. 2001. Coupling an advanced land surface-hydrology model with the Penn State–NCAR MM5 modeling system. Part I: model implementation and sensitivity. *Mon. Weather Rev.* **129**, 569–585.

Chen, L., Liang, X. Z., DeWitt, D., Samel, A. N. and Wang, J. X. L. 2016. Simulation of seasonal US precipitation and temperature by the nested CWRF-ECHAM system. *Clim. Dynam.* **46**, 879–896.

Cocke, S., LaRow, T. E. and Shin, D. W. 2007. Seasonal rainfall predictions over the southeast United States using the Florida State University nested regional spectral model. *J. Geophys. Res.* **112**, D04106.

Dai, A. 2006. Precipitation characteristics in eighteen coupled climate models. *J. Climate* **19**, 4605–4630.

Davies, H. C. and Turner, R. E. 1977. Updating prediction models by dynamical relaxation: an examination of the technique. *Q. J. Roy. Meteor. Soc.* **103**, 225–245.

Duan, A., Wu, G., Liu, Y., Ma, Y., Zhao, P. and co-authors. 2012. Weather and climate effects of the Tibetan Plateau. *Adv. Atmos. Sci.* **29**, 978–992.

Dudhia, J. 1989. Numerical study of convection observed during the winter monsoon experiment using a mesoscale two-dimensional model. *J. Atmos. Sci.* **46**, 3077–3107.

Gao, X., Shi, Y., Zhang, D. and Giorgi, F. 2012. Climate change in China in the 21st century as simulated by a high resolution regional climate model. *Chinese Sci. Bull.* **57**, 1188–1195.

Gao, X., Shi, Y., Han, Z., Wang, M., Wu, J. and co-authors. 2017. Performance of RegCM4 over major river basins in China. *Adv. Atmos. Sci.* **34**, 441–455.

Giorgi, F. and Bates, G. T. 1989. The climatological skill of a regional model over complex terrain. *Mon. Weather Rev.* **117**, 2325–2347.

Giorgi, F. and Mearns, L. O. 1999. Introduction to special section: regional climate modeling revisited. *J. Geophys. Res.* **104**, 6335–6352.

Giorgi, F. and Shields, C. 1999. Tests of precipitation parameterizations available in latest version of NCAR regional climate model (RegCM) over continental United States. *J. Geophys. Res.* **104**, 6353–6375.

Gochis, D. J., Shuttleworth, W. J. and Yang, Z.-L. 2002. Sensitivity of the modeled North American monsoon regional climate to convective parameterization. *Mon. Weather Rev.* **130**, 1282–1298.

Grell, G. A. 1993. Prognostic evaluation of assumptions used by cumulus parameterizations. *Mon. Weather Rev.* **121**, 764–787.

Hall, A. and Qu, X. 2006. Using the current seasonal cycle to constrain snow albedo feedback in future climate change. *Geophys. Res. Lett.* **33**, L03502.

Herwehe, J. A., Alapaty, K., Spero, T. L. and Nolte, C. G. 2014. Increasing the credibility of regional climate simulations by introducing subgrid-scale cloud-radiation interactions. *J. Geophys. Res.* **119**, 5317–5330.

Hong, S. and Lim, J. 2006. The WRF single-moment 6-class microphysics scheme (WSM6). *J. Korean Meteorol. Soc.* **42**, 129–151.

Huang, D. Q., Zhu, J., Zhang, Y. C. and Huang, A. N. 2013. Uncertainties on the simulated summer precipitation over Eastern China from the CMIP5 models. *J. Geophys. Res. Atmos.* **118**, 9035–9047.

Jiang, Z., Li, W., Xu, J. and Li, L. 2015. Extreme precipitation indices over China in CMIP5 models. Part I: model evaluation. *J. Climate* **28**, 8603–8619.

Kain, J. S. 2004. The Kain-Fritsch convective parameterization: an update. *J. Appl. Meteorol.* **43**, 170–181.

Kanamitsu, M., Ebisuzaki, W., Woollen, J., Yang, S. K., Hnilo, J. J. and co-authors. 2002. NCEP–DOE AMIP-II reanalysis (R-2). *Bull. Am. Meteorol. Soc.* **83**, 1631–1643.

Kang, I. S., Jin, K., Wang, B., Lau, K. M., Shukla, J. and co-authors. 2002. Intercomparison of the climatological variations of Asian summer monsoon precipitation simulated by 10 GCMs. *Clim. Dynam.* **19**, 383–395.

Kitoh, A., Endo, H., Krishna Kumar, K., Cavalcanti, I. F. A., Goswami, P. and co-authors. 2013. Monsoons in a changing world: a regional perspective in a global context. *J. Geophys. Res.* **118**, 3053–3065.

Lee, D.-K., Cha, D.-H. and Choi, S.-J. 2005. A sensitivity study of regional climate simulation to convective parameterization schemes for 1998 East Asian summer monsoon. *Terr. Atmopheric Ocean. Sci.* **16**, 989–1015.

Li, J., Zhang, Q., Chen, Y. D. and Singh, V. P. 2013. GCMs-based spatiotemporal evolution of climate extremes during the 21st century in China. *J. Geophys. Res. Atmos.* **118**, 11017–11035.

Liang, X.-Z., Li, L., Kunkel, K. E., Ting, M. and Wang, J. X. L. 2004. Regional climate model simulation of U.S. precipitation during 1982–2002. Part I: annual cycle. *J. Climate* **17**, 3510–3529.

Liang, X.-Z., Xu, M., Kunkel, K. E., Grell, G. A. and Kain, J. S. 2007. Regional climate model simulation of U.S.–Mexico summer precipitation using the optimal ensemble of two cumulus parameterizations. *J. Climate* **20**, 5201–5207.

Liu, S., Gao, W., Xu, M., Wang, X. and Liang, X. Z. 2009. China summer precipitation simulations using an optimal ensemble of cumulus schemes. *Front. Earth Sci. China* **3**, 248–257.

Mlawer, E. J., Taubman, S. J., Brown, P. D., Iacono, M. J. and Clough, S. A. 1997. Radiative transfer for inhomogeneous atmospheres:

RRTM, a validated correlated-k model for the longwave. *J. Geophys. Res. Atmos.* **102**, 16663–16682.

Noh, Y., Cheon, W., Hong, S. and Raasch, S. 2003. Improvement of the K-profile model for the planetary boundary layer based on large eddy simulation data. *Bound-layer. Meteorol.* **107**, 401–427.

Qiao, F. and Liang, X. Z. 2014. Effects of cumulus parameterizations on predictions of summer flood in the Central United States. *Clim. Dynam.* **45**, 727–744.

Ratna, S. B., Ratnam, J. V., Behera, S. K., Rautenbach, C. J. d., Ndarana, T. and co-authors. 2014. Performance assessment of three convective parameterization schemes in WRF for downscaling summer rainfall over South Africa. *Clim. Dynam.* **42**, 2931–2953.

Ratnam, J. V. and Krishna Kumar, K. 2005. Sensitivity of the simulated monsoons of 1987 and 1988 to convective parameterization schemes in MM5. *J. Climate* **18**, 2724–2743.

Reynolds, R. W., Rayner, N. A., Smith, T. M., Stokes, D. C. and Wang, W. 2002. An improved *in situ* and satellite SST analysis for climate. *J. Climate* **15**, 1609–1625.

Skamarock, W. C., Klemp, J. B., Dudhi, J., Gill, D. O., Barker, D. M. and co-authors. 2008. A description of the advanced research WRF version 3. *NCAR Tech. Note NCAR/TN-475+STR*, 113 pp.

Taylor, K. E. 2001. Summarizing multiple aspects of model performance in a single diagram. *J. Geophys. Res.* **106**, 7183–7192.

Xu, J. and Small, E. E. 2002. Simulating summertime rainfall variability in the North American monsoon region: the influence of convection and radiation parameterizations. *J. Geophys. Res. Atmos.* **107**, 4727–4743.

Xu, Y., Gao, X., Shen, Y., Xu, C., Shi, Y. and co-authors. 2009. A daily temperature dataset over China and its application in validating a RCM simulation. *Adv. Atmos. Sci.* **26**, 763–772.

Yang, H., Jiang, Z. and Li, L. 2016. Biases and improvements in three dynamical downscaling climate simulations over China. *Clim. Dynam.* **47**, 3235–3251.

Yu, E., Wang, H., Gao, Y. and Sun, J. 2011. Impacts of cumulus convective parameterization schemes on summer monsoon precipitation simulation over China. *Acta Meteorol. Sinica* **25**, 581–592.

Yu, E., Sun, J., Chen, H. and Xiang, W. 2015. Evaluation of a high-resolution historical simulation over China: climatology and extremes. *Clim. Dynam.* **45**, 2013–2031.

Zhang, X., Alexander, L., Hegerl, G. C., Jones, P., Tank, A. K. and co-authors. 2011. Indices for monitoring changes in extremes based on daily temperature and precipitation data. *Wiley Interdiscip. Rev. Clim. Chang.* **2**, 851–870.

Zhou, T. and Yu, R. 2006. Twentieth-century surface air temperature over China and the globe simulated by coupled climate models. *J. Climate* **19**, 5843–5858.

Zhou, J. L., Tits, A. L. and Lawrence, C. T. 1997. User's guide for FFSQP version 3.7: A FORTRAN code for solving constrained nonlinear (minimax) optimization problems, generating iterates satisfying all inequality and linear constraint. Institute for Systems Research, University of Maryland. *Tech. Rep. SRC-TR-92-107r5*, 44 pp.

Zhou, T., Yu, R., Li, H. and Wang, B. 2008. Ocean forcing to changes in global monsoon precipitation over the recent half-century. *J. Climate* **21**, 3833–3852.